Parallel Imaging: The Basics

Peter Kellman
Laboratory of Cardiac Energetics, NHLBI, National Institutes of Health, DHHS, Bethesda, MD, USA 20892
kellman@nih.gov

1. Introduction

Parallel imaging exploits the difference in sensitivities between individual coil elements in a receive array to reduce the number of gradient encoding steps required for imaging. Parallel imaging was originally conceived [1-3] as a means of ultrafast imaging using a single echo readout, replacing gradient phase encoding entirely with spatial encoding using the coil sensitivities. However, it soon became apparent that there were fundamental as well as practical limitations to the effective number of encodes that were possible. This led to more realistic implementations [4-6] which used gradient phase encoding with a reduced number of steps, referred to as sub-encoding. This tutorial will give an overview of the basic parallel MR imaging problem formulation and solutions for both image and *k*-space domain implementations.

As shown in the simplified illustration of Figure 1, an array of receive coils with sensitivities, $s_i(x,y,z)$ are used to acquire signals G_i from the sample volume with magnetization f(x,y,z). In the early published parallel MR literature, the signals $G_i(k_x) = \sum_{x,y} s_i(x,y) f(x,y) e^{-jk_x x}$ consisted of a single readout (i.e, frequency encoded but without gradient encoding). The encoding (or forward problem) which was a combination of frequency encoding, $e^{-jk_x x}$, and spatial coil sensitivity encoding, $s_i(x,y,z)$, may be represented in matrix form $\mathbf{G} = \mathbf{Sf}$ after discretization. The desired magnetization image f(x,y) may be reconstructed by solving the inverse problem, $\mathbf{f} = \mathbf{S}^{-1}\mathbf{G}$. Unique solution of the inverse problem requires that the number of independent equations (i.e., unique coils) is equal to the number of unknowns, in this case number of y-values; with a greater number of equations (coils) the system of equations becomes over-determined and has a least squares solution or pseudo-inverse. Due to limitation on the number of coils which are effectively independent, multiple gradient encoding steps are employed in practice as described in the remainder of the tutorial.

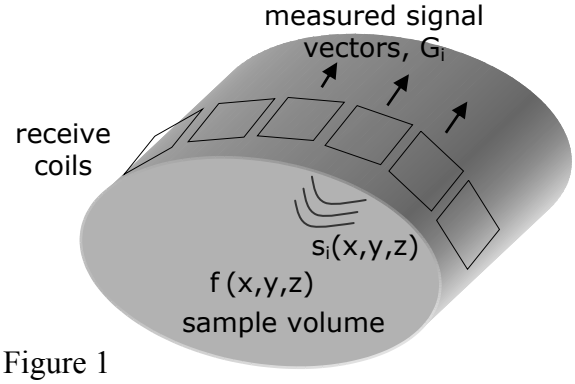

Figure 1

The chronology of parallel MR imaging is summarized in Fig. 2 using approximate dates. Following initial conceptual papers [1-6], practical implementations of parallel MR were presented by Sodickson and Manning [7] and Pruessmann, *et al*. [12]. Sodickson, et al. [7,8] proposed a method known as SiMultaneous Acquisition of Spatial Harmonics (SMASH) which is a *k*-space implementation of parallel MR imaging. Pruessmann *et al*. presented a general formulation and performance analysis of the image domain sensitivity encoding method (SENSE). A number of generalizations and extensions have been reported. The SMASH method has been generalized to provide tailored harmonic fits [9], coil-by-coil image reconstruction [10], and a generalized matrix formulation [11]. SENSE has been applied to arbitrary *k*-space trajectories [13] and has been extended to 2-d SENSE [14] and multi-slice parallel acquisitions [15]. General analysis frameworks for comparing image and *k*-space domain implementations, as well as hybrids, are presented in [16-17]. References on array signal processing [18-20] formulate the problem as an optimization with nulling constraints.

- Basic Parallel MR Concept (1987-1990)
  phase array combining
  sensitivity encoding & hybrids (sub-encoding)
- Practical implementations (1997-1999)
  SMASH: k-space approach
  SENSE: image domain
- Optimization (1999-current)
  auto-calibration
  matrix inverse conditioning
  coil optimization
- Extensions (2000-current)
  generalized SMASH
  2-d SENSE & multi-slice
  arbitrary k-space
- Applications (2000-current)

Figure 2. Chronology of parallel MR imaging

A key area of current research has been on auto-calibration methods for estimating the in-vivo coil sensitivities [21-26]. Optimizations include the numerical conditioning or regularization of the matrix inverse [27-30], and the design of coil arrays for parallel MR imaging [31-34]. Research and development has led to an improved understanding of performance limitations such as tradeoffs between acceleration, # coils, and SNR degradation. Advances in technology have led to practical implementation and numerous applications have been proposed and demonstrated.

The presentation will begin with the general matrix formulation of combined sensitivity and Fourier (gradient) encoding (the forward problem) and the inverse solution for arbitrary *k*-space. This general formulation will then be simplified to the case of Cartesian *k*-space acquisition. Equivalence between image and *k*-space domain implementations will be discussed and the concept of coil sensitivity spectra [16] will be presented to motivate how missing gradient encodes (views) are replaced by parallel MR. The methods of SMASH and harmonic fitting are then presented. SNR losses are inherent in inverse problems due to ill-conditioning. The variance inflation factor, or so called SENSE g-factor [12], is explained. The method of 2-d SENSE [14] has been proposed for improved g-factor for volume imaging with high acceleration factors. The 2-d SENSE method is briefly described. Thoughout the presentation, it is assumed that the coils sensitivities, s_i are known or can be estimated. The subject of in vivo estimation of coil sensitivities and auto-calibration are presented at the conclusion.

2. Matrix Formulation

The matrix formulation (Eq. [1]) and solution (following Pruessmann, *et al*. [12]) incorporates both Fourier (gradient) and coil sensitivity encoding for arbitrary *k*-space acquisition. In this formulation the matrix-vector notation assumes that 2d variables are ordered in a 1-d vector. In other words, the column vector $\mathbf{r}$ consists of $n_r=N^2$ elements over (x,y), and likewise, $\mathbf{k}$, assumes n_k values over (k_x,k_y). The column vector $\mathbf{G}$ consists of measured *k*-space data for n_c coils, i.e., n_c n_k x1. Eq. 1 represents the encoding or forward problem.

$$G_i(\mathbf{k}) = \sum_{\mathbf{r}} s_i(\mathbf{r}) e^{-j\mathbf{kr}} f(\mathbf{r}) + n_i(\mathbf{k})$$

$$\mathbf{G} = \mathbf{E}\mathbf{f} + \mathbf{n} \qquad [1]$$

$s_i(\mathbf{r})$	complex coil sensitivities (B_1-maps) for coil i=1,…,n_c
$\mathbf{r}$	position vector $\mathbf{r}=[r_1,r_2, \ldots r_{n_r}]$
$\mathbf{k}$	*k*-space sample vector $\mathbf{k}=[k_1,k_2, \ldots k_{n_k}]$
$\mathbf{G}$	vector of measured k-space samples ($n_c n_k$ x 1)
$\mathbf{E}$	encoding matrix ($n_c n_k$ x N^2)
$\mathbf{f}$	vector of magnetization image voxels (N^2x1)
n_i	noise for coil i

Thoughout the presentation, it is assumed that the coils sensitivities, s_i are known or can be estimated with sufficient accuracy. The subject of in vivo estimation of coil sensitivities is very important and will be addressed briefly at the conclusion. The encoding functions for combined Fourier (gradient) and coil sensitivity encoding are shown in Fig. 3 for illustration purposes. In this simulated illustration, there are 4 coils surrounding a cylindrical phantom and Fourier encoding is shown for (k_x,k_y)= (0,0), (2,0), (0,2), and (2,2). The real encoding functions (images) are shown.

$$\hat{\mathbf{f}} = \left(\mathbf{E}^H \Psi^{-1} \mathbf{E}\right)^{-1} \mathbf{E}^H \Psi^{-1} \mathbf{G}$$

$$\Psi = \mathrm{cov}(\mathbf{n}) = E\{\mathbf{n}\mathbf{n}^H\} \qquad [2]$$

The image reconstruction or solution to the inverse problem (Eq. [2]) may be estimated by the least squares method provided the total number of encodes n_c n_k > n_r =N^2. Parallel imaging may be used to achieve acceleration by using fewer gradient encoding steps (n_k) and still maintain the same spatial resolution. The noise covariance (Ψ) weighted least squares solution optimizes the SNR subject to the constraint of nulling artifacts due to undersampling. The solution for this arbitrary *k*-space formulation requires an N^2xN^2 matrix inversion which is impractical to implement with direct inversion for typical image sizes (e.g., 256x256). The least square solution [13] based on the iterative conjugate gradient method may be used to compute solutions converging within reasonable reconstruction times. An example short axis cardiac image reconstructed using the iterative conjugate gradient method is shown in Fig. 4 for the 1st 6 iterations. In this example, a variable density Cartesian *k*-space acquisition was used with an acquisition matrix of 128x60 and 35 phase encodes acquired, every other line with 5 added center lines. The acquisition used a real-time true-FISP sequence without ECG triggering, and corresponded to a frame rate of approximately 15 fps.

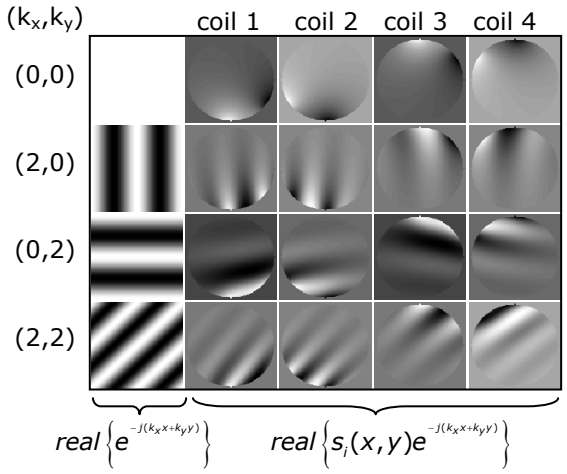

Figure 3. Example encoding functions

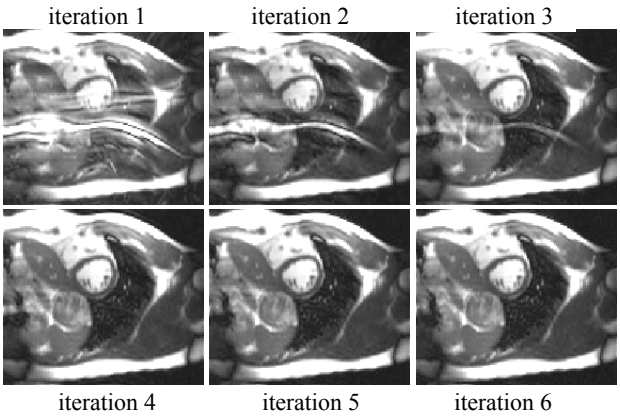

Figure 4. Example short axis cardiac images using variable density Cartesian *k*-space acquisition, reconstructed using iterative conjugate gradient SENSE.

The simplified matrix formulation for uniform Cartesian *k*-space acquisition is presented next. Figure 5 illustrates the aliasing due to uniformly undersampled Cartesian acquisition for rate R=2 showing images from a single coil. Given knowledge of the coil sensitivities, the aliased images can be separated by solving linear equations. The matrix formulation and solution are given in Equation 3. **S** is referred to as the coil sensitivity matrix, and **U** is the unmixing matrix. Application of the SENSE unmixing matrix may be equivalently described as phased array combining as illustrated in Figure 6. Example short axis cardiac images acquired at acceleration rates 2, 3, and 4 are shown in Figure 7 before and after SENSE reconstruction. These are real-time free breathing true-FISP without ECG triggering acquired at 15, 22.5, and 30 fps for rates 2, 3, and 4 respectively, using a 128x60 acquisition matrix.

$$\begin{bmatrix} g_1(x,y) \\ \vdots \\ g_N(x,y) \end{bmatrix} = \begin{bmatrix} s_1(x,y) & s_1(x,y-FOV/2) \\ \vdots & \vdots \\ s_N(x,y) & s_N(x,y-FOV/2) \end{bmatrix} \begin{bmatrix} f(x,y) \\ f(x,y-FOV/2) \end{bmatrix} + \begin{bmatrix} n_1(x,y) \\ \vdots \\ n_N(x,y) \end{bmatrix} \quad [3]$$

$$\mathbf{g} = \mathbf{S}\mathbf{f} + \mathbf{n}$$

$$\hat{\mathbf{f}} = \left(\mathbf{S}^H \Psi^{-1} \mathbf{S}\right)^{-1} \mathbf{S}^H \Psi^{-1} \mathbf{g} = \mathbf{U}\mathbf{g}$$

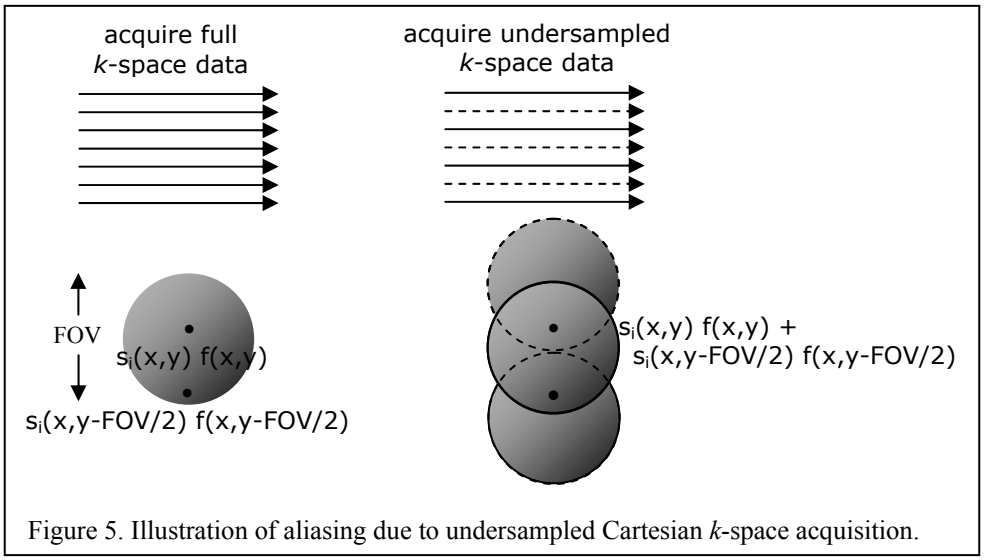

Figure 5. Illustration of aliasing due to undersampled Cartesian *k*-space acquisition.

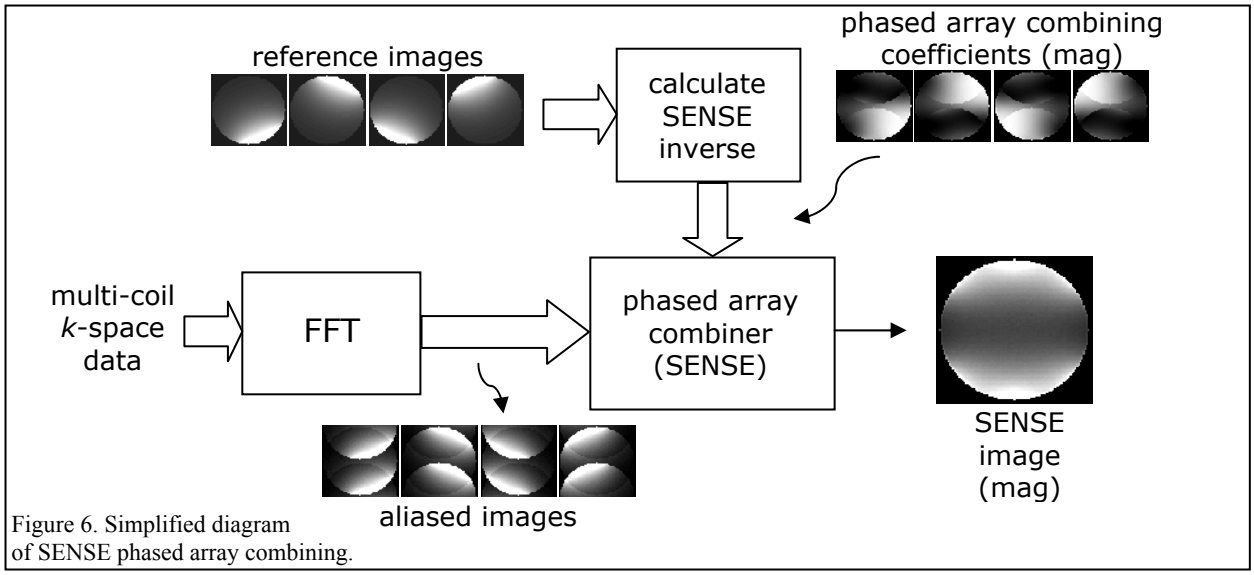

Figure 6. Simplified diagram of SENSE phased array combining.

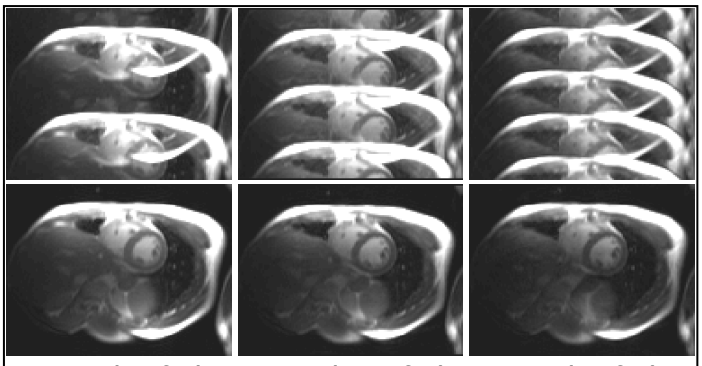

Figure 7. Example short axis cardiac SENSE images.

Image domain phased array combining may equivalently be performed in the *k*-space domain as shown in Fig. 8, where image domain multiplication by $u_i(x,y)$ has been implemented by *k*-space domain convolution with $\mathcal{U}_i(k_x,k_y)$. This leads directly to *k*-space methods such as SMASH which fill the missing *k*-space using convolution with a truncated kernel composed of a set of 1 or more harmonic fits to the coil sensitivities. Further insight is gained [16] by examining the spatial spectra of the coil sensitivities illustrated in Fig 9. The non-uniform coil sensitivity profile leads to a blurring in *k*-space, which allows parallel imaging to solve for the missing phase encodes.

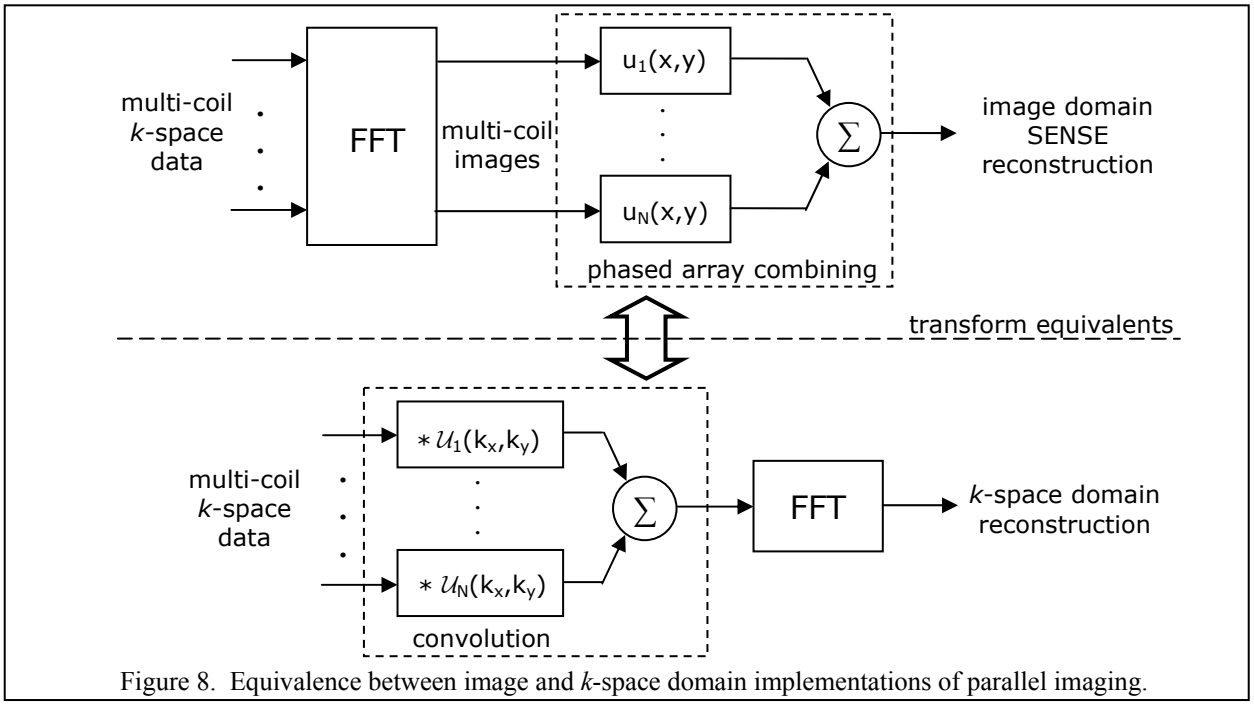

Figure 8. Equivalence between image and *k*-space domain implementations of parallel imaging.

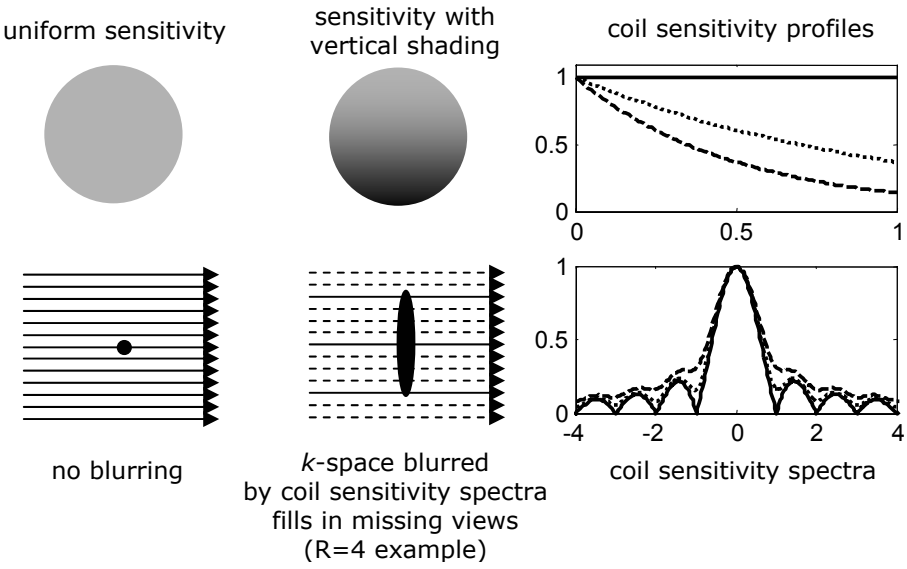

Figure 9. Coil sensitivity "spectra" illustrating *k*-space view filling concept.

In the formulation of the *k*-space parallel imaging method for Cartesian *k*-space acquisition, the acquired *k*-space data may be written as:

$$G_i(k_x,k_y) = \sum_{x,y} s_i(x,y)e^{-j(k_x x,k_y y)} f(x,y) + n_i(k_x,k_y) \quad [4]$$

and the SMASH estimate of the "composite" *k*-space data with missing views filled in may be written as:

$$\hat{G}(k_x,k_y - m\Delta k_y) = \sum_i n_i^{(m)} G_i(k_x,k_y) \quad [5]$$

where the coefficients $n_i^{(m)}$ are calculated by a fit to the *m*-th harmonic.

$$\sum_i n_i^{(m)} s_i(x,y) \approx e^{jm\Delta k_y y} \quad [6]$$

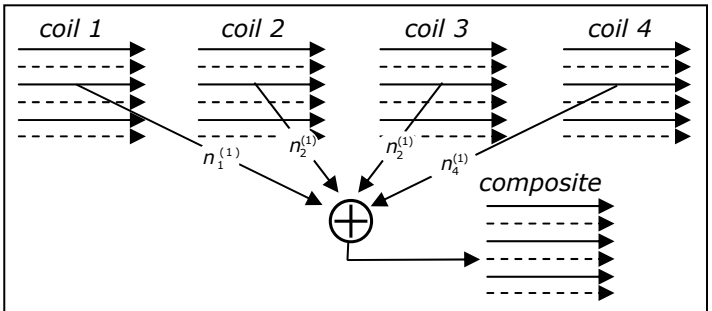

Figure 10. SMASH procedure for filling missing *k*-space lines.

This procedure is diagrammed in the illustration of Fig. 10. The harmonic fits for m=0 and m=1 are shown in Fig. 11 for simulated complex coil profiles. There is considerable error between the actual and desired harmonic fits. The error may be greatly reduced by using a "tailored" harmonic fit [9] which fits to a weighted set of harmonics, as illustrated in Fig. 12 which uses a phased sum of the complex coils as a weighting function, as described by Eq. 7.

$$\sum_i n_i^{(m)} s_i(x,y) \approx s_0(x,y)e^{jm\Delta k_y y}$$
$$s_0(x,y) = \sum_{i=1}^{Nc} s_i(x,y)e^{j\phi_i} \text{ phased sum} \quad [7]$$

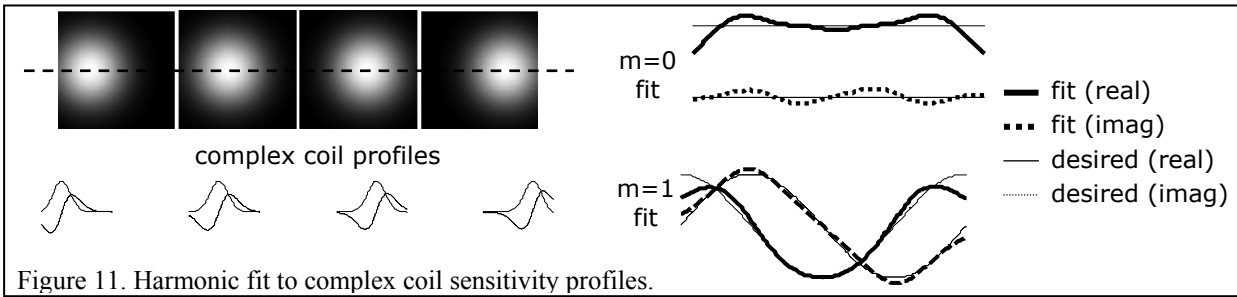

Figure 11. Harmonic fit to complex coil sensitivity profiles.

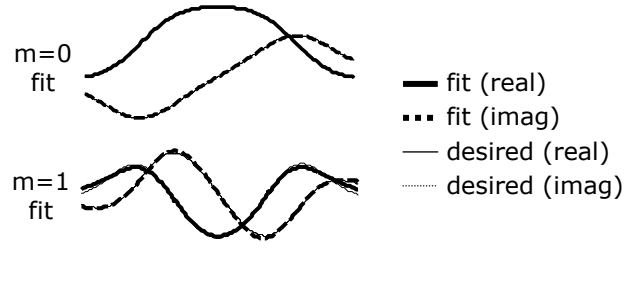

Figure 12. Tailored harmonic fit to complex coil sensitivities profiles.

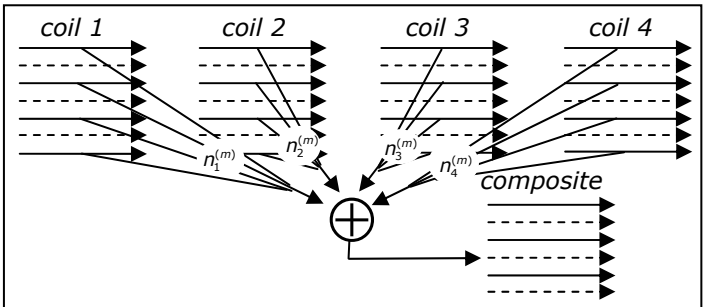

Figure 13. SMASH procedure using block of *k*-space lines.

A further generalization of the SMASH method is to use blocks of *k*-space lines for calculating the missing phase encodes, as shown in Fig. 13. This improves the ability to model coil sensitivity profiles which have sharper edges, and correspondingly greater spatial bandwidth. For example, this approach is used in the GRAPPA method [23].

3. SNR losses

Accelerated imaging using the SENSE method incurs a loss in SNR due to both reduced imaging time and sub-optimal coil geometry (the so called g-factor). The SNR for accelerated parallel imaging using the SENSE method may be calculated as:

$$SNR_{SENSE} = SNR_{optimum} \Big/ g\sqrt{R} \ , \qquad [8]$$

where R is the acceleration factor and $SNR_{optimum}$ is the SNR for B_1-weighted optimum phased array combining [18] and the loss in SNR due to variance inflation, SENSE *g*-factor [12], is defined as:

$$g_k(x,y) = \frac{1}{\sqrt{(\mathbf{S}^{\mathrm{H}}\Psi^{-1}\mathbf{S})^{-1}_{(k,k)}(\mathbf{S}^{\mathrm{H}}\Psi^{-1}\mathbf{S})_{(k,k)}}} \ , \qquad [9]$$

where the subscript *(k,k)* denotes the index of the matrix corresponding to the *k*-th sub-image. The spatially varying *g*-factor represents the loss in SNR (inflation in variance) due to ill-conditioning of the matrix inverse, which depends on the acceleration rate, the number of coils, specific coil sensitivity profiles (sizes, shapes, and positions), slice orientation, and phase encode direction.

The *g*-factor depends strongly on position (x,y,z) and has several hotspots. Figures 14 and 15 show maps of the *g*-factor for 4 and 8 coils, respectively, at various acceleration rates.

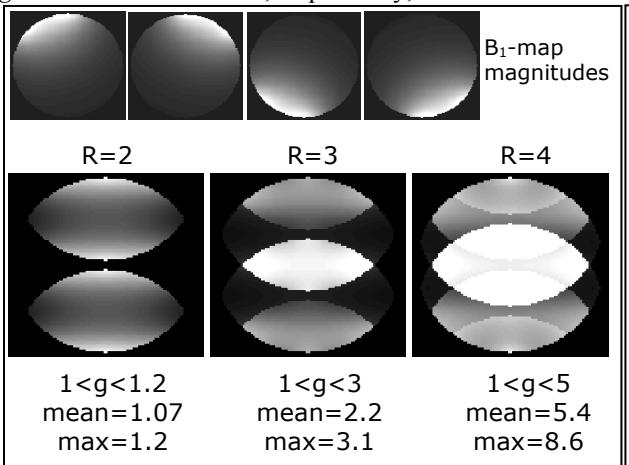

Fig. 14. Example g-factor maps for SENSE with 4-coils.

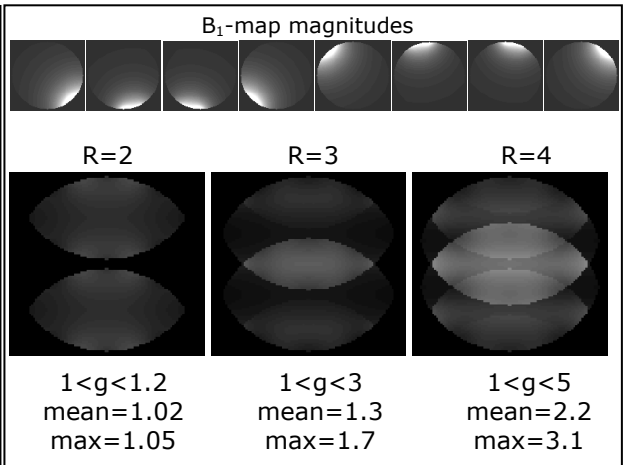

Fig. 15. Example g-factor maps for SENSE with 8-coils.

The ill-conditioning of the inverse also increases the effect of errors in estimates of the complex coil sensitivities (B_1-maps). Errors in the sensitivity matrix will degrade the alias artifact suppression. It is customary to regularize or condition the matrix inverse [27-30]. Adaptive regularization may be used to spatially vary the degree of conditioning and dramatically improve the SENSE reconstruction.

4. 2-d SENSE

In volume imaging applications using 2 phase encode dimensions (or spectroscopic imaging), it may be preferable to perform accelerated imaging in each of the 2 phase encode directions rather than a higher rate along a single direction. This has been referred to as 2-d SENSE [14]. The matrix formulation for the case of R=2 acceleration along y and z, for an overall R=4 acceleration, is written as:

$$\begin{bmatrix} g_1(x,y,z) \\ \vdots \\ g_N(x,y,z) \end{bmatrix} = \begin{bmatrix} s_1(x,y,z) & s_1(x,y-D_y,z) & s_1(x,y,z-D_z) & s_1(x,y-D_y,z-D_z) \\ \vdots & & & \vdots \\ s_N(x,y,z) & s_N(x,y-D_y,z) & s_N(x,y,z-D_z) & s_N(x,y-D_y,z-D_z) \end{bmatrix} \begin{bmatrix} f(x,y,z) \\ f(x,y-D_y,z) \\ f(x,y,z-D_z) \\ f(x,y-D_y,z-D_z) \end{bmatrix} + \begin{bmatrix} n_1(x,y,z) \\ \vdots \\ n_N(x,y,z) \end{bmatrix} \quad [10]$$

where $D_y=FOV_y/2$ and $D_z=FOV_z/2$. Depending on the specific coil sensitivity profiles and slice geometry, it may be possible to achieve a *g*-factor which is greatly reduced when compared with R=4 acceleration along a single dimension, e.g., y or z in this case. A scheme for performing SENSE with multi-slice parallel acquisition is presented in [15].

5. B_1-Map Estimates and Auto-calibration

Thoughout the presentation, it is assumed that the coils sensitivities, s_i are known or can be estimated with sufficient accuracy. The complex coil sensitivities, also known as B_1-maps, depend not only on the coil geometry and orientation, but are stongly influenced by the sample volume of interest which alters the magnetic field distribution. For this reason, in-vivo estimation of coil sensitivities is key to achieving accurate estimates. In the case of *k*-space methods such as auto-SMASH and GRAPPA [21-23], B_1-maps are not explicitly calculated. Rather, *k*-space weighting coefficients are based on in vivo *k*-space reference data directly, as described briefly at the conclusion of this section.

In vivo B_1-maps may be estimated from separate or interleaved reference scans, or from the undersampled imaging data itself in a variety of schemes referred to as auto-calibrating. A basic description follows. The complete process may often involve several additional steps to include spatial smoothing and sometimes extrapolation, the details of which are not fully described. First, the raw sensitivities are estimated from the individual coil images acquired without undersampling artifacts, at either full or reduced spatial resolution. Normalization with either a body coil image or root-sum-of-squares (RSS) combined magnitude image is used to remove the image modulus, as described by Eq. [11] or [12], respectively, where the subscript i designates the coil index. In the case of normalization with a body coil image, both the modulus and phase of the object are removed, assuming that the body coil sensitivity is uniform. In the case of normalization by RSS magnitude image only the image modulus is removed leaving the object phase, f/|f|. Furthermore, the raw sensitivies will be weighted by the combined magnitude image leading to a weighting on the final parallel MR reconstructed image. The object phase may be removed using an array processing scheme based on the sample correlation matrix and dominant eigenvector [19]. The object phase may have rapid spatial variation, and removal of this phase enables spatial smoothing of the raw sensitivities. Example images and raw sensitivity estimates are shown in Fig. 16 for a cardiac imaging application.

$$\hat{s}_i(x,y) = \hat{f}_i(x,y) \Big/ f_{\text{body coil}}(x,y) \approx \frac{s_i(x,y)\ f(x,y)}{s_{\text{body coil}}(x,y)\ f(x,y)} = \frac{s_i(x,y)}{s_{\text{body coil}}(x,y)} \propto s_i(x,y) \quad [11]$$

$$\hat{s}_i(x,y) = \hat{f}_i(x,y) \Big/ \sqrt{\sum_i \left|\hat{f}_i(x,y)\right|^2} \approx \frac{s_i(x,y)\ f(x,y)}{\sqrt{\sum_i \left|s_i(x,y)\ f(x,y)\right|^2}} \approx \frac{s_i(x,y)}{\sqrt{\sum_i \left|s_i(x,y)\right|^2}} \left[\frac{f(x,y)}{|f(x,y)|}\right] \quad [12]$$

Since the coil sensitivities generally have slower spatial variation than the object being imaged, several implementations acquire the B1-map data at lower spatial resolution or employ spatial smoothing to reduce noise or fluctuations. If separate unaccelerated scans are used to acquire reference images, reduced resolution is often used to acquire the images in a reasonable time period.

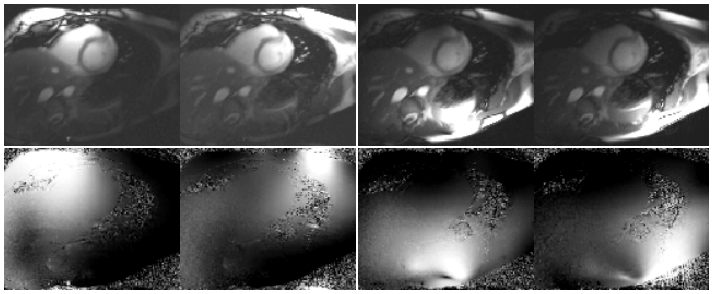

Figure. 16. Individual coil images (top row) and raw sensitivities (bottom row) per Eq.[12].

Auto-calibration in which reference data are acquired coincident with the imaging have the benefit of adapting to changes in position of coil or body that might otherwise occur between calibration and imaging. Several auto-calibrating methods are based on acquiring additional *k*-space center lines each time frame [21-24] or by using non-Cartesian sampling such as radial *k*-space acquisition which naturally oversamples the center of *k*-space. The central *k*-space data is then used to reconstruct low resolution images for each coil which are used to estimate sensitivity maps at each imaging time frame. For example, Fig. 17 illustrates the lines of *k*-space acquired for Cartesian sampling with variable density. The acquisition of center lines reduces the net acceleration rate, although they may be used with a generalized reconstruction (see Fig. 4) to slightly improve the image quality. The lower resolution of the reference will limit the accuracy of the sensitivity maps which may lead to residual artifacts. Reconstruction of lower resolution reference images may require additional windowing to reduce artifacts arising from Gibb's ringing in the sensitivity maps [24].

In dynamic imaging applications, it is possible to aquire a full spatial resolution reference image suitable for auto-calibration by using a time interleaved *k*-space acquisition as illustrated in Fig. 18 (rate, R=2 example). Multiple undersampled frames may be averaged or low pass temporally filtered to reconstruct a low temporal resolution reference image used to calculate coil sensitivities. This method known as TSENSE [25] is diagrammed in Fig. 19. Integration or temporal filtering may be implemented equivalently in either *k*-space or image domains with appropriate zero-filling of missing data.

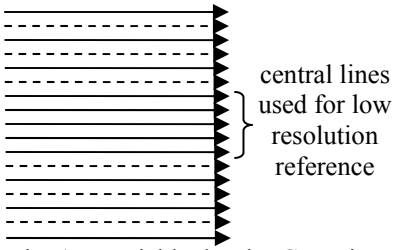

Fig. 17. Variable density Cartesian *k*-space acquisition.

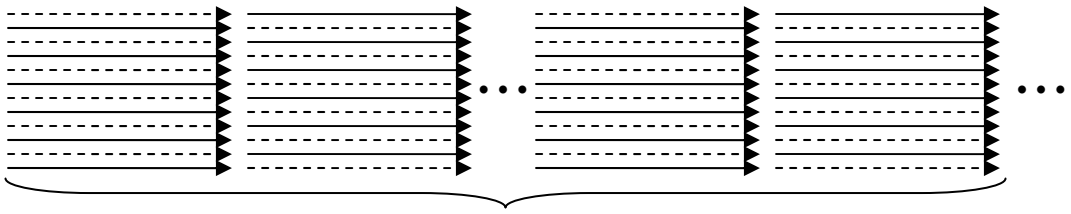

Fig. 18. Example of time interleaved *k*-space acquisition used for auto-calibrating TSENSE method.

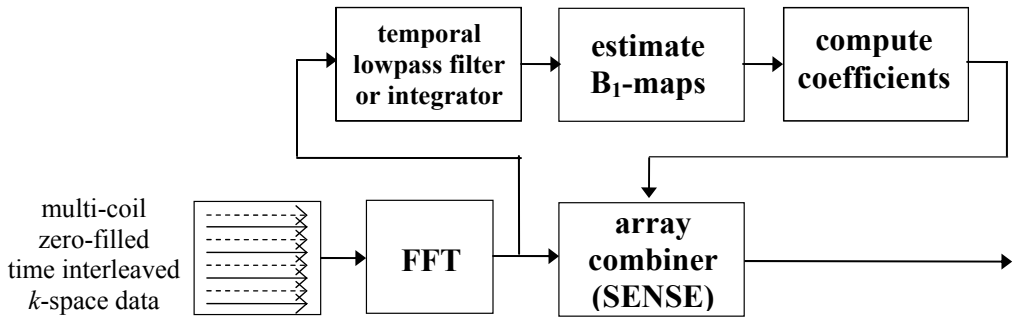

Fig. 19. Simplified diagram for auto-calibrating TSENSE method.

K-space methods such as auto-SMASH, variable density auto-SMASH, and GRAPPA [21-23] are auto-calibrating methods which utilize additionally acquired central *k*-space lines, also known as auto-calibration signal (ACS) lines, to calculate the coefficients $n_i^{(m)}$ used for SMASH reconstruction. These coefficients are calculated directly from the *k*-space data without explicitly calculating sensitivity maps. In the original auto-SMASH formulation the coefficients were calculated by least squares fit as:

$$\sum_i S_i^{ACS}(k_y - m\Delta k_y) = \sum_i n_i^{(m)} S_i(k_y) \quad [13]$$

where $S_i(k_y)$ is the *k*-space data for phase encode line k_y and *i* represents the coil index. In variable density auto-SMASH the fit may be performed for multiple pairs of ACS lines,

$$\sum_i S_i^{ACS}(k_y - (m+l)\Delta k_y) = \sum_i n_{i,l}^{(m)} S_i(k_y - l\Delta k_y) \quad [14]$$

and the multiple fits $n_{i,l}^{(m)}$ cans be combined with a weighted average based on the signal energy, where *l* represents the number of available fits. The GRAPPA method [23] performs parallel MR reconstructions for each coil and uses root-sum-of-squares combining to produce a magnitude image. It further generalizes the reconstruction by using a block (or sliding block) fit for each coil *j*,

$$S_j^{ACS}(k_y - (m+l)\Delta k_y) = \sum_i \sum_b n_{i,j,l,b}^{(m)} S_i(k_y - (bR+l)\Delta k_y) \quad [15]$$

where *R* denotes the acceleration rate, *b* is the index of the undersampled line within each block, and *l* represents the number of available fits. GRAPPA, as well as VD auto-SMASH, use a variable density sampling to acquire the ACS lines each time frame. For dynamic imaging application, GRAPPA may be implemented with a time interleaved undersampled acquisition and derive the ACS lines by temporal averaging. This approach is referred to as TGRAPPA [26] and has the benefits of improved speed and image quality due to increased block size and coefficient averaging.

6. References

Early References

[1] Carlson JW. An algorithm for NMR imaging reconstruction based on multiple RF receiver coils. *J Magn Reson* 1987:74:376-380.

[2] Hutchinson M, Raff U. Fast MRI data acquisition using multiple detectors. *Magn Reson Med* 1988:6(1):87-91.

[3] Kwiat D, Einav S, Navon G. A decoupled coil detector array for fast image acquisition in magnetic resonance imaging. *Med Phys* 1991:18(2):251-65.

[4] Kelton JR, Magin RL, Wright SM. An algorithm for rapid image acquisition using multiple receiver coils. *Eighth Annual Meeting of the Society for Magnetic Resonance in Medicine*. Amsterdam, Netherlands, 1989:1172.

[5] Carlson JW, Minemura T. Imaging time reduction through multiple receiver coil data acquisition and image reconstruction. *Magn Reson Med* 1993:29(5):681-7.

[6] Ra JB, Rim CY. Fast imaging using subencoding data sets from multiple detectors. *Magn Reson Med* 1993:30(1):142-5.

SMASH

[7] Sodickson DK, Manning WJ. Simultaneous acquisition of spatial harmonics (SMASH): fast imaging with radiofrequency coil arrays. *Magn Reson Med* 1997:38(4):591-603.

[8] Sodickson DK, Griswold MA, Jakob PM, Edelman RR, Manning WJ. Signal-to-noise ratio and signal-to-noise efficiency in SMASH imaging. *Magn. Reson. Med.* 41, 1009-1022 (1999).

[9] Sodickson DK. Tailored SMASH image reconstructions for robust in vivo parallel MR imaging. *Magn. Reson. Med.* 44, 243-251 (2000).

[10] McKenzie CA, Ohliger MA, Yeh EN, Price MD, Sodickson DK. Coil-by-coil image reconstruction with SMASH. *Magn Reson Med*. 2001 Sep;46(3):619-23.

[11] Bydder M, Larkman DJ, Hajnal JV. Generalized SMASH imaging. *Magn Reson Med* 2002 Jan;47(1):160-70.

SENSE

[12] Pruessmann KP, Weiger M, Scheidegger MB, Boesiger P. SENSE: Sensitivity encoding for fast MRI. *Magn Reson Med* 1999:42(5):952-962.

[13] Pruessmann KP, Weiger M, Bornert P, Boesiger P. Advances in sensitivity encoding with arbitrary k-space trajectories. *Magn Reson Med* 2001:46(4):638-51.

2-d SENSE
[14] Weiger M, Pruessmann KP, Boesiger P. 2D SENSE for faster 3D MRI. *MAGMA*. 2002 Mar;14(1):10-9.
[15] Larkman DJ, Hajnal JV, Herlihy AH, Coutts GA, Young IR, Ehnholm G. Use of multicoil arrays for separation of signal from multiple slices simultaneously excited. *J Magn Reson Imaging*. 2001 Feb;13(2):313-7.

General methods
[16] Wang Y. Description of Parallel Imaging in MRI using multiple coils. *Magn Reson Med*. 2000 Sep;44:495-9.
[17] Sodickson DK, McKenzie CA. A Generalized Approach to Parallel Magnetic Resonance Imaging. *Med Phys* 2001;28(8):1629-1643.

Array Processing
[18] Roemer PB, Edelstein WA, Hayes CE, Souza SP, Mueller OM. The NMR phased array. *Magn Reson Med* 1990;16:192–225.
[19] Walsh DO, Gmitro AF, Marcellin MW. Adaptive reconstruction of phased array MR imagery. *Magn Reson Med* 2000;43:682–690.
[20] Johnson DH, Dudgeon DE. Array signal processing: concepts and techniques. Englewood Cliffs, NJ: Prentiss-Hall; 1993. 355–371.

Auto-calibration
[21] Jakob PM, Griswold MA, Edelman RR, Sodickson DK. AUTO-SMASH: a self-calibrating technique for SMASH imaging. *MAGMA* 1998;7:42-54.
[22] Heidemann RM, Griswold MA, Haase A, Jakob PM. VD-AUTO-SMASH imaging. *Magn Reson Med* 2001:45(6):1066-74.
[23] Griswold MA, Jakob PM, Heidemann RM, Nittka M, Jellus V, Wang J, Kiefer B, Haase A. Generalized autocalibrating partially parallel acquisitions (GRAPPA). *Magn Reson Med*. 2002 Jun;47(6):1202-10.
[24] McKenzie CA, Yeh EN, Ohliger MA, Price MD, Sodickson DK. Self-calibrating parallel imaging with automatic coil sensitivity extraction. *Magn Reson Med*. 2002 Mar;47(3):529-38.
[25] Kellman P, Epstein FH, McVeigh ER, Adaptive sensitivity encoding incorporating temporal filtering (TSENSE). *Magn Reson Med*. 2001 May; 45(5):846-52.
[26] Breuer F, Kellman P, Griswold MA, Jakob PM. Dynamic Autocalibrated Parallel Imaging using TGRAPPA. *Proc. Eleventh Scientific Meeting Intl. Soc. Magn Reson Med* 2003; 2330.

Matrix Conditioning & Regularization
[27] King KF, Angelos L. SENSE image quality improvement using matrix regularization. *Proc. Ninth Scientific Meeting Intl. Soc. Magn Reson Med* 2001;1771.
[28] Kellman P, McVeigh ER. SENSE Coefficient Calculation using Adaptive Regularization. *ISMRM Workshop on Minimum MR Data Acquisition Methods*. Marco Island, Florida Oct. 2001.
[29] Liang ZP, Bammer R, Ji J, Pelc NJ, Glover GH. Making Better SENSE: Wavelet Denoising, Tikhonov Regularization, and Total Least Squares. *Proc. Tenth Scientific Meeting Intl. Soc. Magn Reson Med* 2002; 2388.
[30] Tsao J, Pruessmann KP, Boesiger P. Feedback Regularization for SENSE Reconstruction. *Proc. Tenth Scientific Meeting Intl. Soc. Magn Reson Med* 2002; 739.

Coils
[31] Griswold MA, Jakob PM, Edelman RR, Sodickson DK. A Multicoil Array Designed for Cardiac SMASH Imaging. *MAGMA* 2000:10:105-113.
[32] Bankson JA, Griswold MA, Wright SM, Sodickson DK. SMASH Imaging with an Eight Element Multiplexed RF Coil Array. *MAGMA* 2000:10:93-104.
[33] Weiger M, Pruessmann KP, Leussler C, Roschmann P, Boesiger P. Specific coil design for SENSE: a six-element cardiac array. *Magn Reson Med* 2001:45(3):495-504.
[34] de Zwart JA, Ledden PJ, Kellman P, van Gelderen P, Duyn JH. Design of a SENSE-Optimized High-Sensitivity MRI Receive Coil for Brain Imaging. *Magn Reson Med*. 2002 Jun; 47(6):1218-27.